Supporting Information

Characterisation of organic solid forms and real-time *in-situ* monitoring of their transformations using solid-state fluorescence

Mathieu Frenette, Gonzalo Cosa* and Tomislav Friščić*

McGill University, Department of Chemistry, H3A 0B8 Montreal, Canada. Fax:+1-514-398-3757; Tel: +1-514-398-3959; E-mail: tomislav.friscic@mcgill.ca; gonzalo.cosa@mcgill.ca

Table of contents

1.1 Experimental

Crystalline indomethacin was obtained from Enzo Life Sciences, Inc. and used as received. For certain crystallization experiments, indomethacin from Aldrich was also used as received. Both Aldrich and Enzo indomethacin had similar fluorescence behaviour and powder X-ray diffraction patterns corresponding to the crystalline γ-form. Fluorescence measurements were performed on a Biotek Synergy 2 multi-mode microplate reader using clear polystyrene 96-well microplates. Room temperature powder X-ray diffraction (PXRD) patterns were collected using a Bruker D2 Phaser powder diffractometer equipped with a CuK_α (λ=1.54060 Å) source, nickel filetr and a Lynxeye detector. DSC measurements were conducted on a TA instruments Q2000 Differential Scanning Calorimeter using a crimped aluminum pan under a constant nitrogen gas flow.

Solid indomethacin that was obtained after recrystallization from ether, known to yield the γ-form,[1,2] exhibited a similar fluorescence emission profile as the commercial Aldrich and Enzo sample. This result confirms that the obtained fluorescence emission from both commercial samples results from γ-indomethacin and not a fluorescent impurity. We note that two hydrolysis/oxidation products of indomethacin—5-methoxy-2-methyl-1H-indole-3-acetic acid and 5-hydroxy-2-methyl-1H-indole-3-acetic acid—are fluorescent in solution and these species were previously used to quantify the presence of indomethacin in blood plasma using HPLC with fluorescence detection.[3]

To obtain the methanol solvate of indomethacin, a saturated solution of indomethacin in boiling methanol was dissolved by further addition of methanol. This solution was allowed to cool, yielding pale yellow long thin needles that were recovered by filtration, washed with cold methanol, dried under mild reduced pressure and kept in a sealed vial at room temperature. The powder X-ray diffraction pattern and differential scanning calorimetry data match previously

reported data for the methanol solvate crystalline form.[5] Water was added to the supernatant of this recrystallization, which immediately formed a white precipitate. Filtration and thorough drying under vacuum yielded the α-form of indomethacin as previously reported.[2]

Amorphous indomethacin was obtained by melting indomethacin in a round-bottom flask at 165-170^{O}C in an atmosphere of argon and pouring the molten liquid into a falcon tube held under liquid nitrogen. The frozen solid was then placed under vacuum in a desiccator to prevent condensation during warming up. Once at room temperature, the sample was lightly triturated using a mortar and pestle. At this point, excess static charge was removed using an antistatic gun (Zerostat). The amorphous and commercial crystalline powders were individually size-separated using a 75 µm and 38 µm mesh grids from Cole Parmer to obtain >75 µm, 38-75 µm and <38 µm particle sized samples. For the calibration curves of fluorescence vs. percent amorphous content, a total weight of 50-100 mg for the appropriate ratio of amorphous and crystalline (γ-form) powder were added in vials, thoroughly mixed using a vortex and ~20 mg were placed in clear-bottom polystyrene 96 well plates. A specially designed plastic plunger with a flat bottom was used to compress the powder; this treatment gave our samples a flat surface and helped us obtain reproducible fluorescence measurements from the top sample surface.

1.2 Fluorescence polarization measurements

Fluorescence intensity measurements were not greatly affected by particle size. For example, the fluorescence intensity of amorphous indomethacin particles smaller than 38 µm and those larger than 75 µm varied by less than 5% of the calibration curve scale

Polarization measurements for crystalline (γ-form) indomethacin were independent of particle size. There was, however, a large effect of particle size on the polarization measurements for the amorphous samples. On clear, freshly prepared films of amorphous indomethacin, the polarization (in mP) could reach ~0.6, while titurated samples ranged around 145 mP, 125 mP and 115 mP for particle sizes greater than 75µm, 38 µm to 75 µm, and smaller than 38 µm, respectively. For this reason, the calibration curve based on polarization measurements was constructed using particles between 38 µm and 75 µm for both crystalline and amorphous starting powders (Fig. S1).

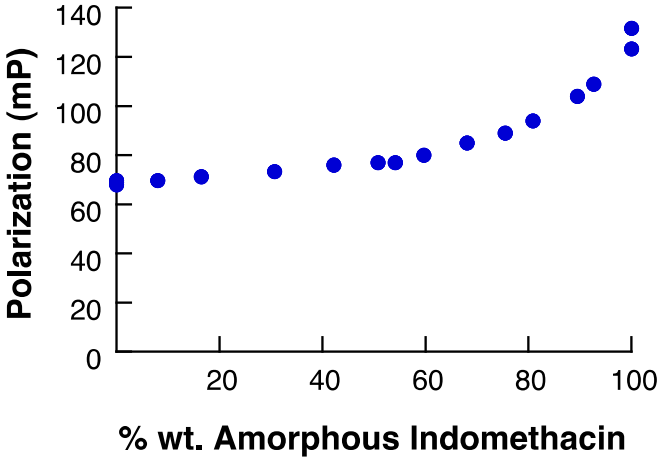

Fig. S1 Fluorescence polarization (excitation 360/40 nm, emission 460/40 nm) of physical mixtures of amorphous and crystalline indomethacin (38-75 mesh). Particles of larger sizes (>75µm) gave similar curve shapes with mP values reaching ~145 for 100% amorphous and smaller particle sizes (<38 µm) gave lower mP values reaching ~115 for 100% amorphous content.

1.3 Differential scanning calorimetry (DSC)

The samples were between 3.5 mg and 5.0 mg in weight. DSC measurements were performed by first cooling the sample to 10 °C, then heating them to 180°C with a constant heating rate of 20°C min^{-1} . The samples were then held at 180 °C for 5 minutes. Results of DSC measurements are shown in Fig. S2 and match those reported previously.[1,4,5]

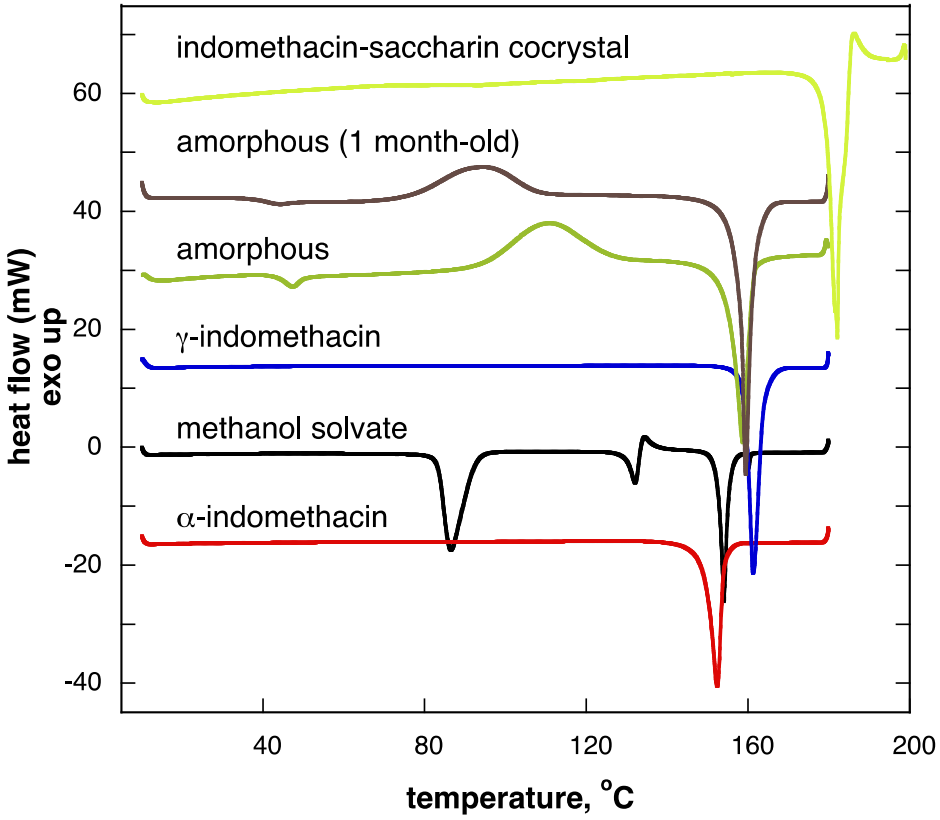

Fig. S2 DSC thermograms of the indicated samples, heated in sealed aluminum pans at a rate of 20°C/min.

1.4 Powder X-ray diffraction (PXRD)

The results of PXRD analysis are shown in Fig. S3 and match those previously reported.[1,4,5] Fluorescence data for an aged amorphous sample (aged at room temperature, sealed vial) is added in Fig. S4 for comparison with the data for freshly prepared amorphous indomethacin and its γ-form.

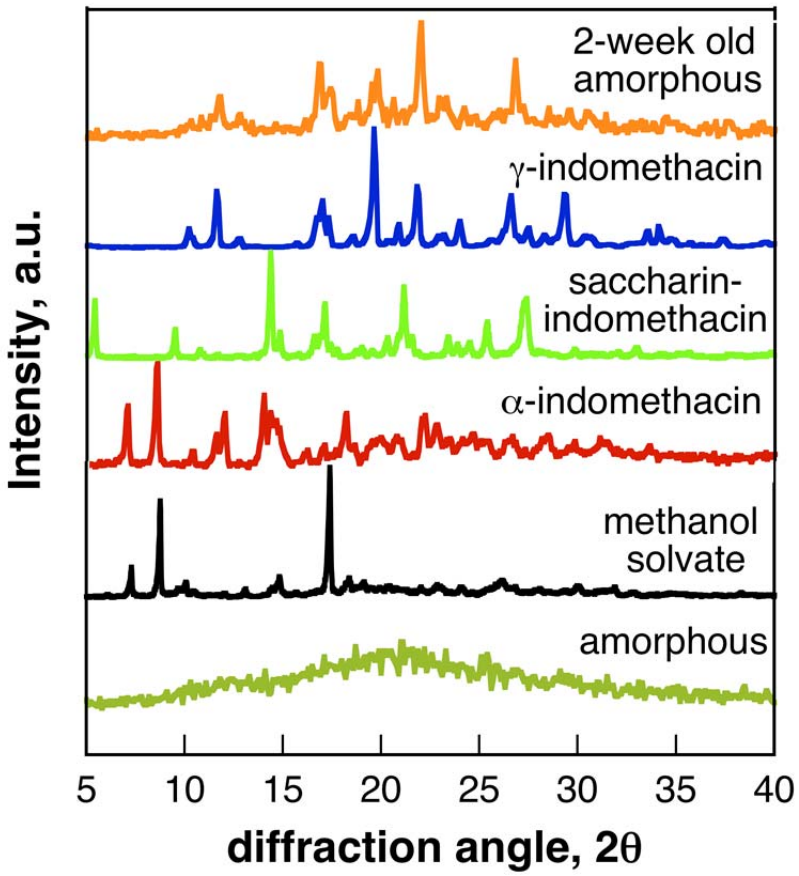

Fig. S3 Powder X-ray diffraction patterns for different solid-state forms of indomethacin.

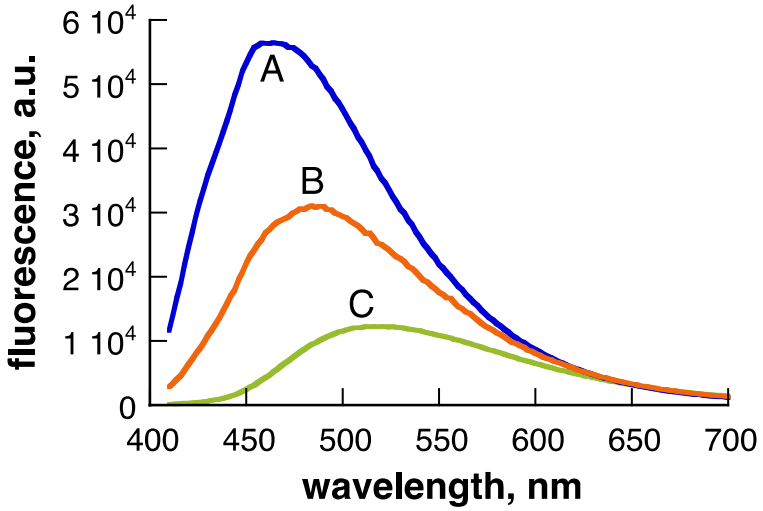

Fig. S4 Fluorescence spectra showing the aging of amorphous using 390 nm excitation (9 nm bandpass) for (A) commercial Enzo sample, (B) 40 day old aged amorphous, (C) freshly prepared amorphous sample.

1.5 Selected examples of solid form transformation kinetics

General comments. The transformation of amorphous to crystalline indomethacin was monitored at 45°C and 100% humidity. Under these conditions, the transformation is rapid and the use of *in situ* measurements proved extremely useful to obtain reliable kinetic measurements and parameters.

For these experiments, freshly prepared amorphous indomethacin (as described above) was size-separated using 75 µm and 53 µm sieves to get >75 µm and 53-75 µm particle sizes. As before, ~ 20 mg of amorphous indomethacin powder was placed in well-plate bottoms and flattened using a plastic pillar with a flat bottom that snugly fit in the well cavity. Crystalline indomethacin (also size-selected) was used as a control and loaded into the same well plate. In the surrounding wells, distilled water was added and a fitting polystyrene lid was placed over the well plate. After temperature equilibration of the plate reader (45°C), the well plate was loaded into the plate reader and kinetics were monitored with the same filter-based excitation and emission wavelengths used to construct the calibration curve from the Fig. 2 inset (360±20 nm and 460±20 nm, respectively). A picture of a well plate after a kinetic run is shown below (Fig. S5).

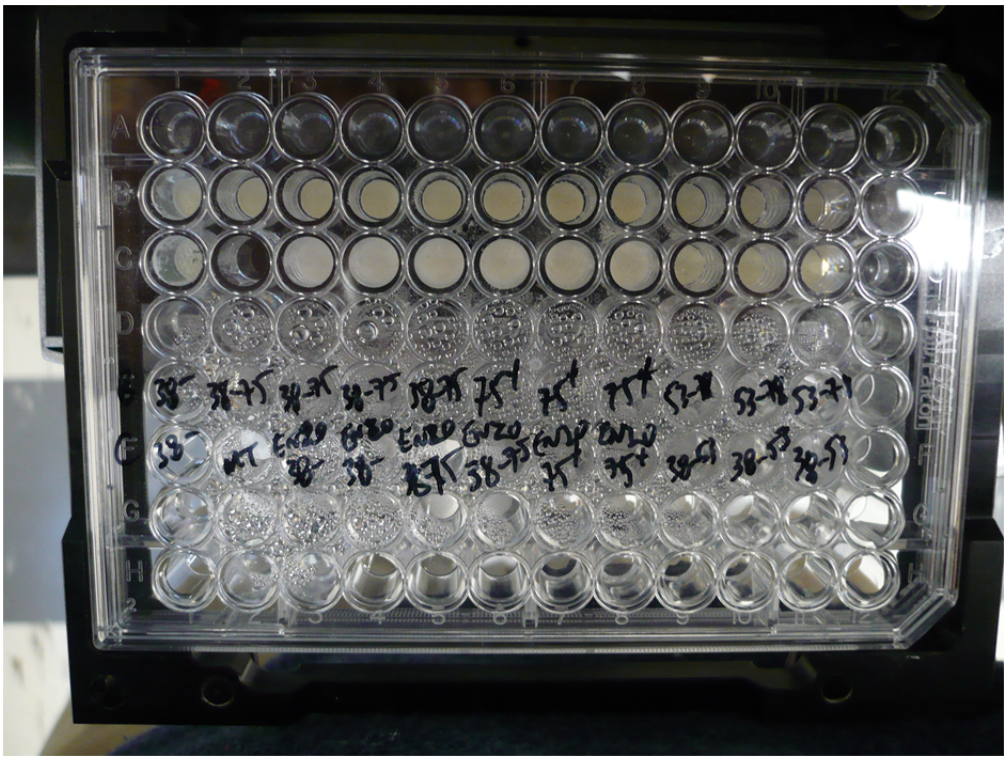

Fig. S5 Clear polystyrene 96-well plate containing size-selected indomethacin (amorphous and γ-form) after a kinetic measurement at 45°C and 100% humidity.

Raw data (shown in Fig. S6) for the amorphous samples were normalized with the 100% γ-form fluorescence intensity measurements to control for temperature dependence on fluorescence intensity and fluctuations in the measurement.

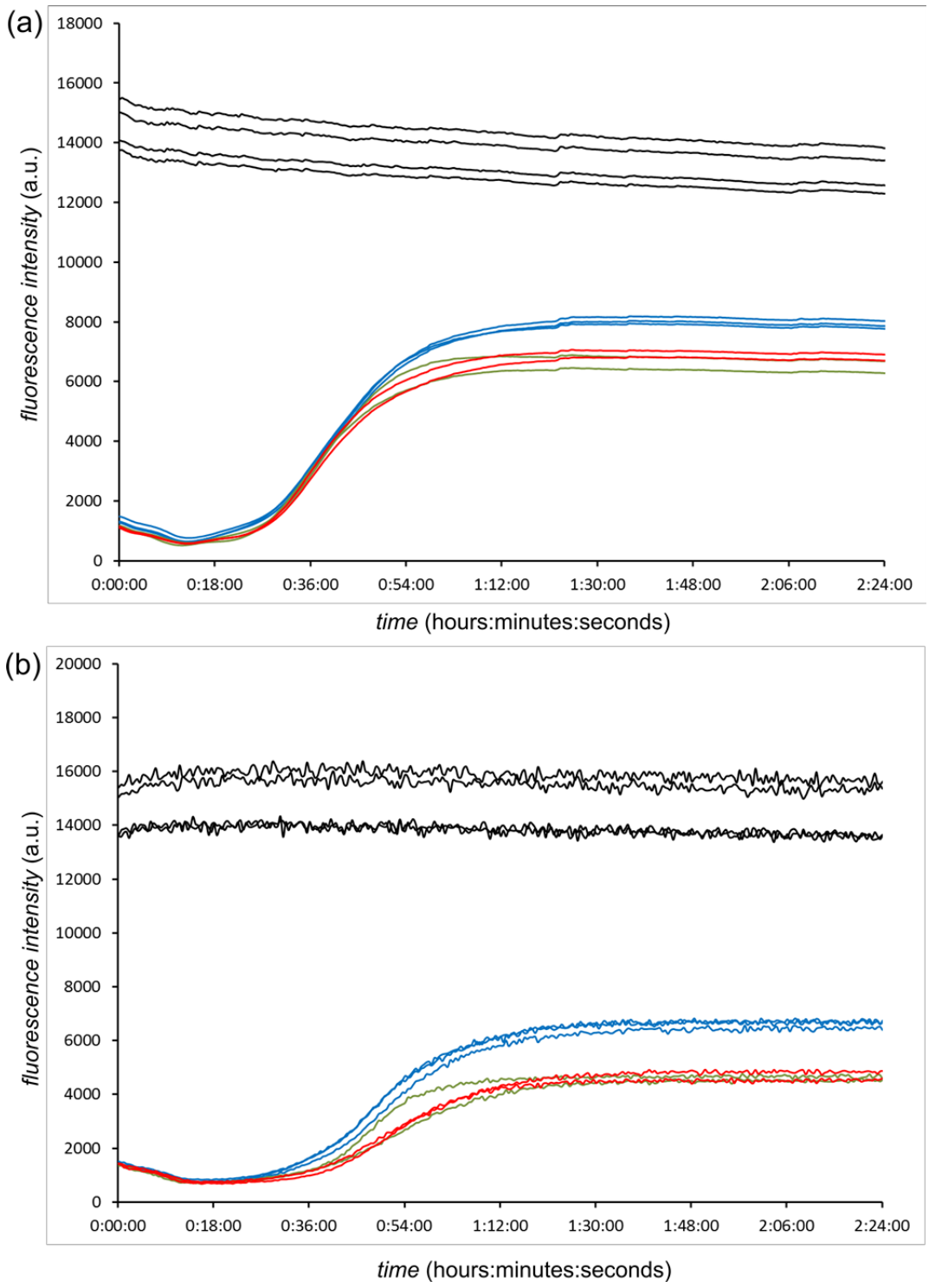

Fig. S6 Raw fluorescence read-out (excitation at 360 ± 20 nm, monitoring at 460 ± 20 nm) for the 45°C, 100% humidity kinetics of amorphous indomethacin: (a) measurements on the top sample surface and (b) measurements on the bottom sample surface. Measurements made on samples with particle size >75 μm are shown in blue, particle size between 53 μm and 75 μm in green and particle size between 38 μm and 53 μm in red. Black line corresponds to concomitant measurements made on samples of γ-indomethacin with particle sizes either between 38 μm and 75 μm, and >75 μm.

The sigmoidal section of the fluorescence emission data for real time in situ reaction monitoring was fitted to a non-linear general JMAEK model, as described in the manuscript.

In addition, the data was also linearised and fitted to 10 well-known models of solid-state transformation kinetics: the JMAEK **A1**, **A2**, **A3** and **A4** models, the Prout-Tompkins **B1** model, the diffusion-controlled **D1**, **D2**, **D3** and **D4** models and the **R1** and **R2** models. For illustration, selected examples of such fits are provided in Figs. S14-S18, and clearly demonstrate that the measured data gives a much better fit to the general JMAEK equation than to any of the 10 alternative models of transformation kinetics. For details of employed kinetic models, see: A. Khawam and D. R. Flanagan, *Solid-state kinetic models: basics and mathematical fundamentals*, *J. Phys. Chem. B*, 2006, **110**, 17315.

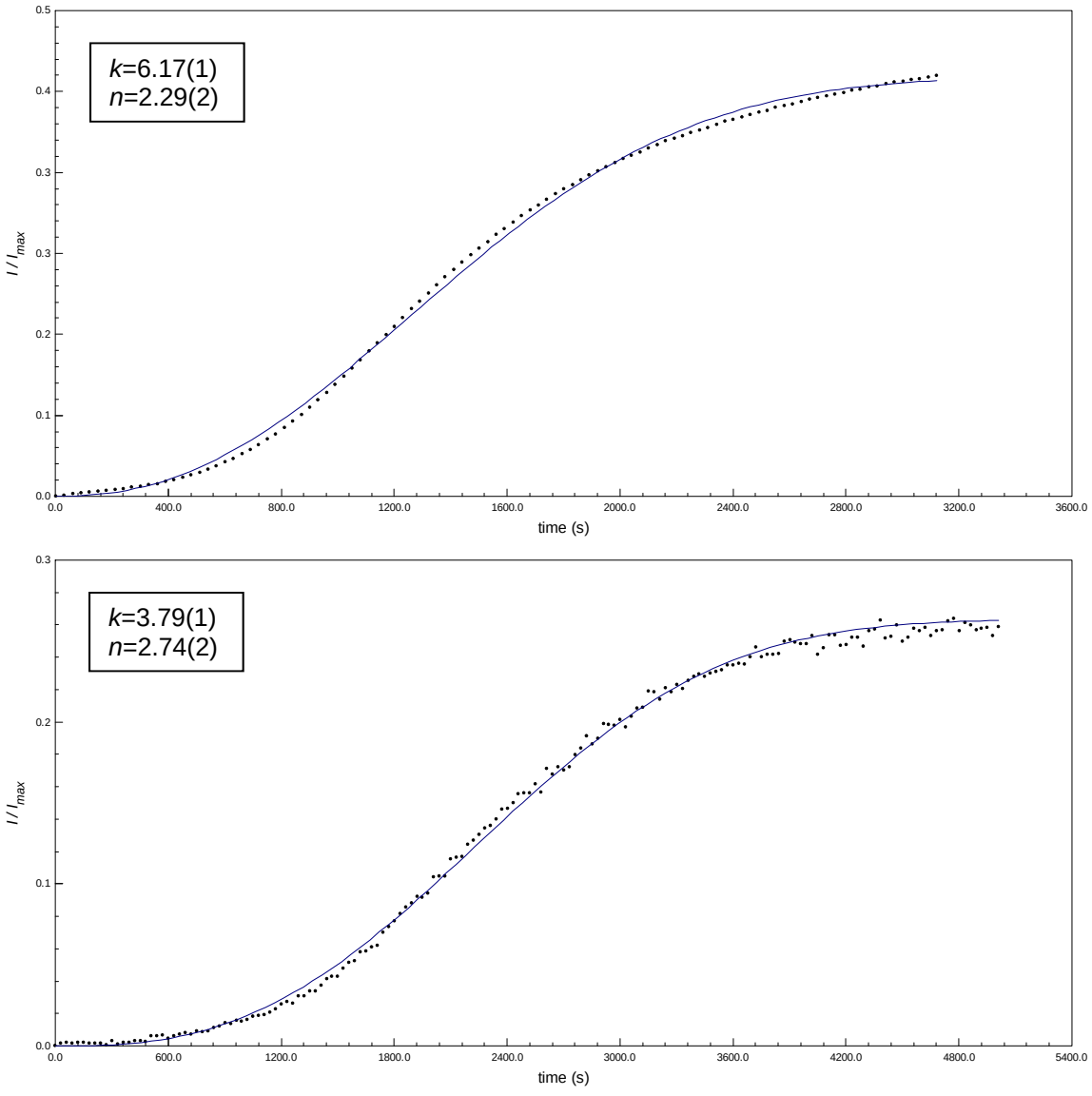

Fig. S7 Non-linear fit of the sigmoidal fluorescence emission data to a general JMAEK model for the transformation of amorphous indomethacin sample with particle size between 38 μm and 53 μm. Fluorescence data was collected from: (top) sample top and (bottom) sample bottom.

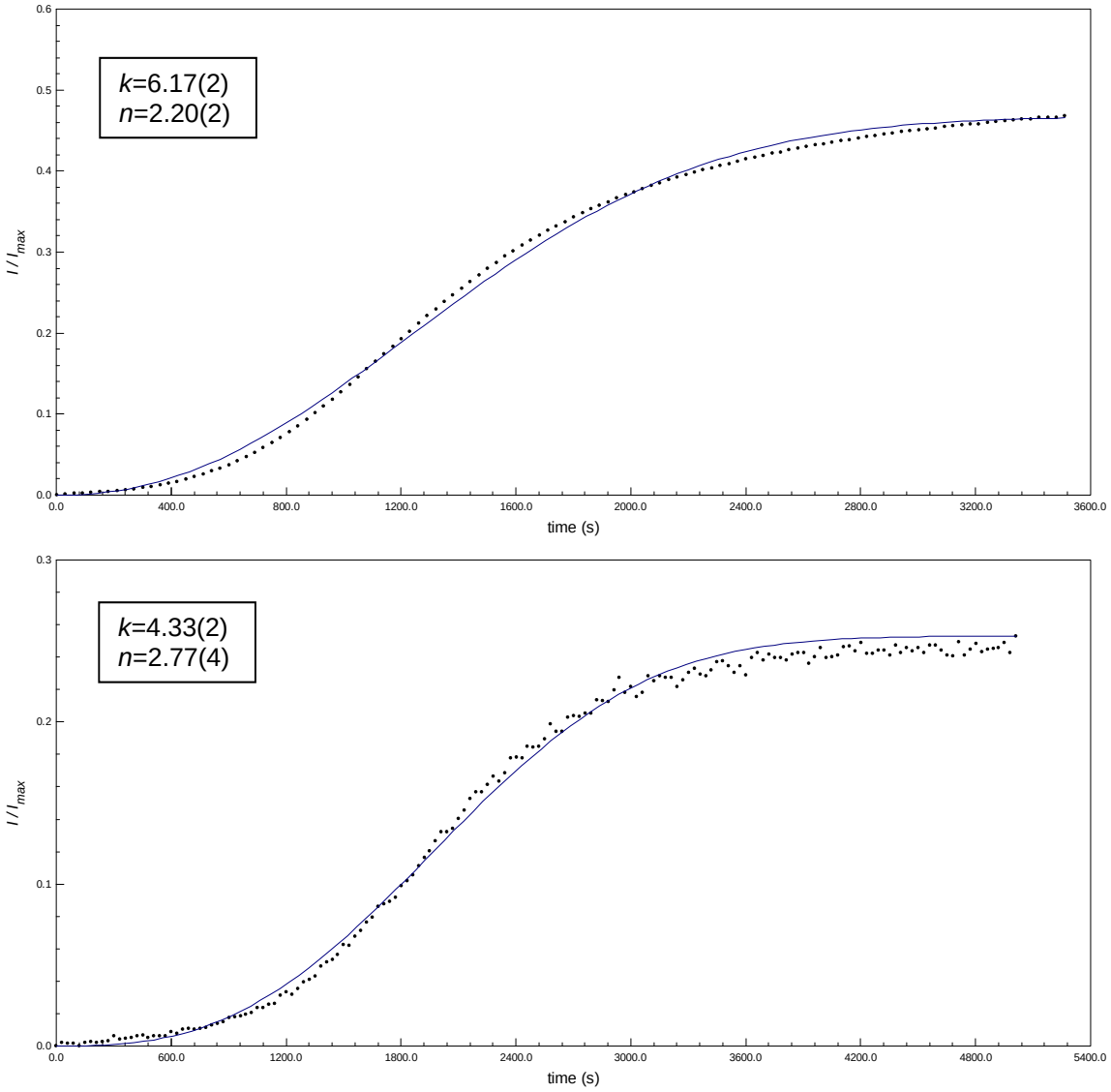

Fig. S8 Non-linear fit of the sigmoidal fluorescence emission data to a general JMAEK model for the transformation of another amorphous indomethacin sample with particle size between 38 μm and 53 μm. Fluorescence data was collected from: (top) sample top and (bottom) sample bottom.

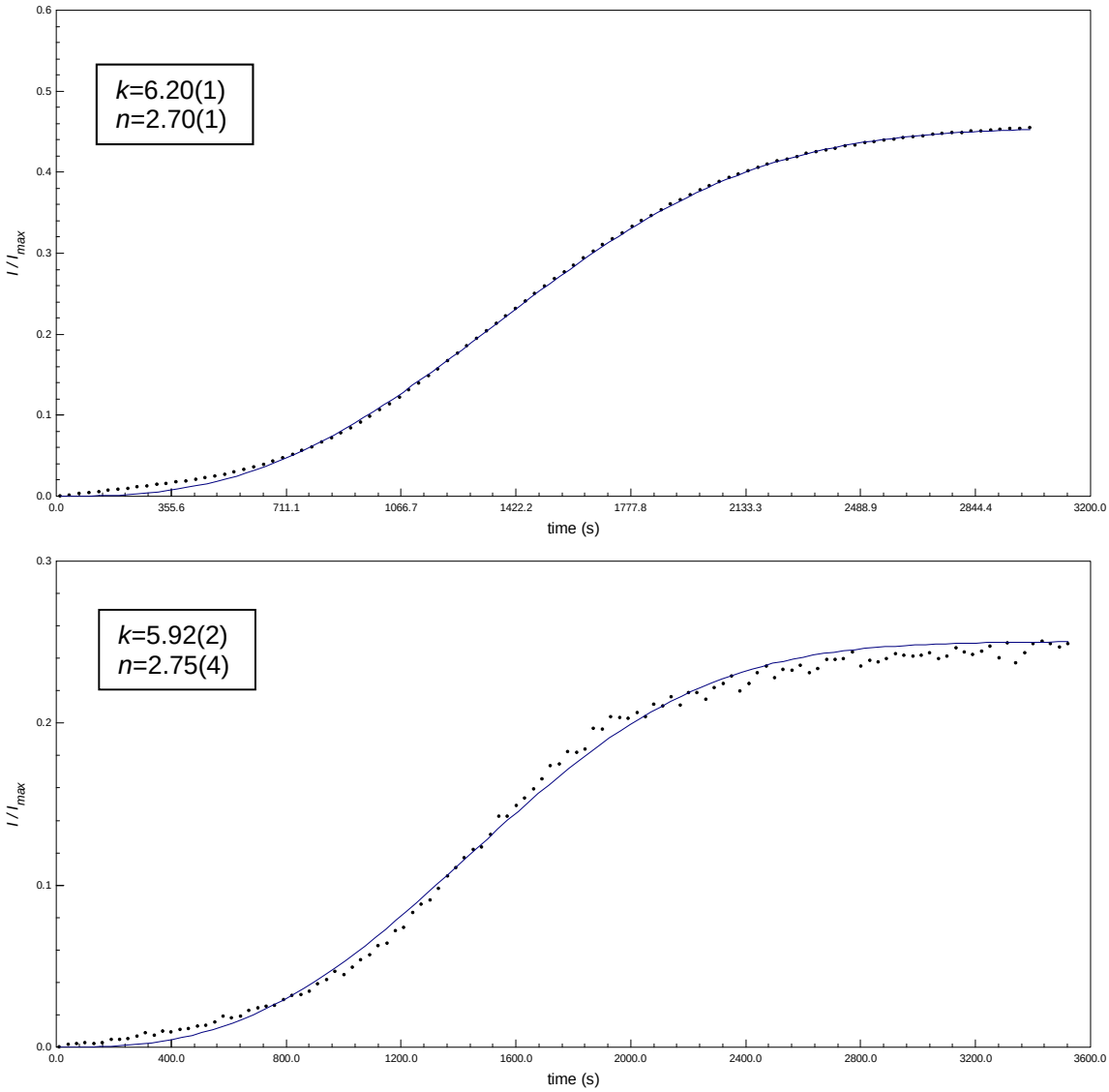

Fig. S9 Non-linear fit of the sigmoidal fluorescence emission data to a general JMAEK model for the transformation of amorphous indomethacin sample with particle size between 53 μm and 75 μm. Fluorescence data was collected from: (top) sample top and (bottom) sample bottom.

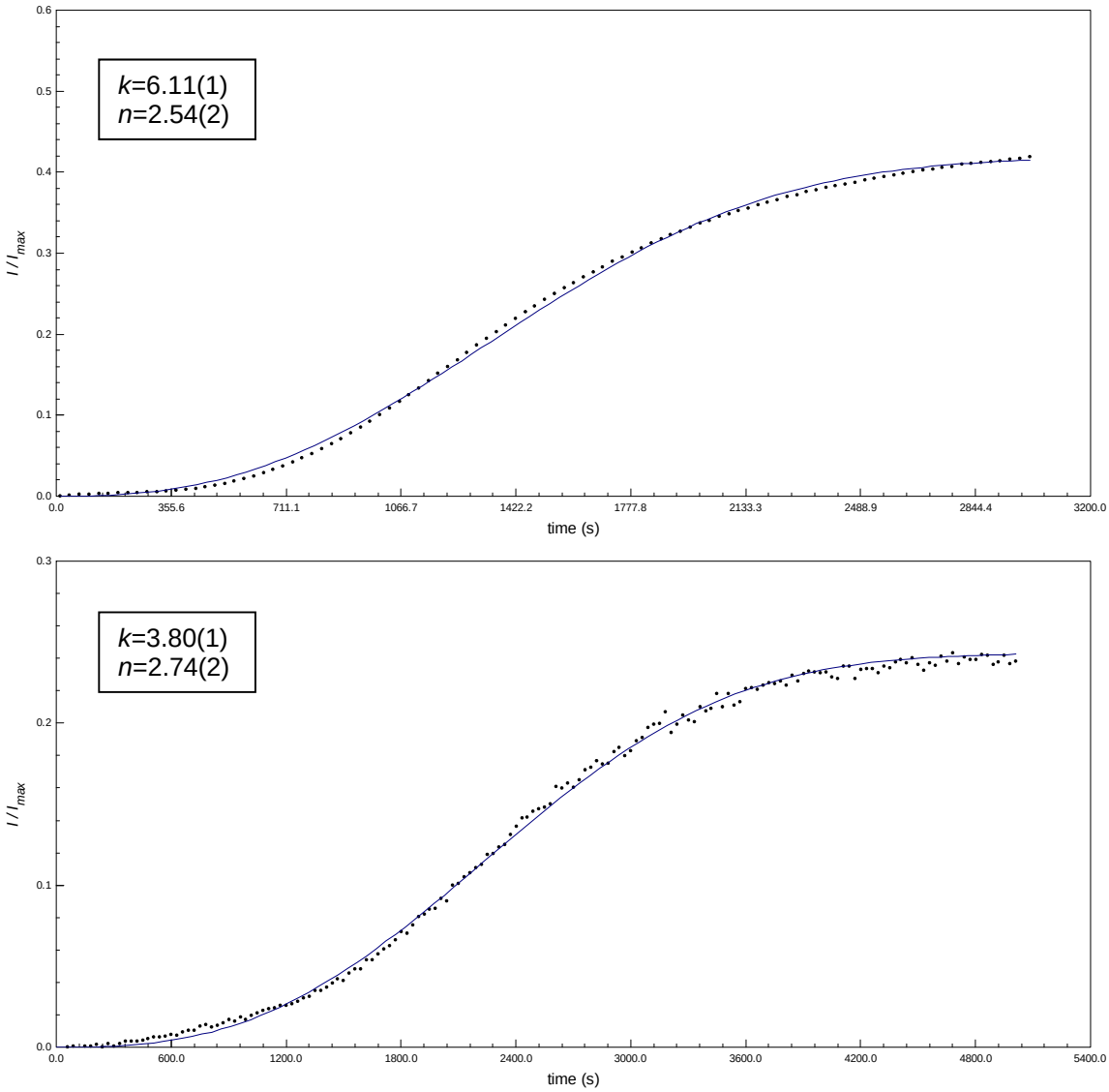

Fig. S10 Non-linear fit of the sigmoidal fluorescence emission data to a general JMAEK model for the transformation of another amorphous indomethacin sample with particle size between 53 μm and 75 μm. Fluorescence data was collected from: (top) sample top and (bottom) sample bottom.

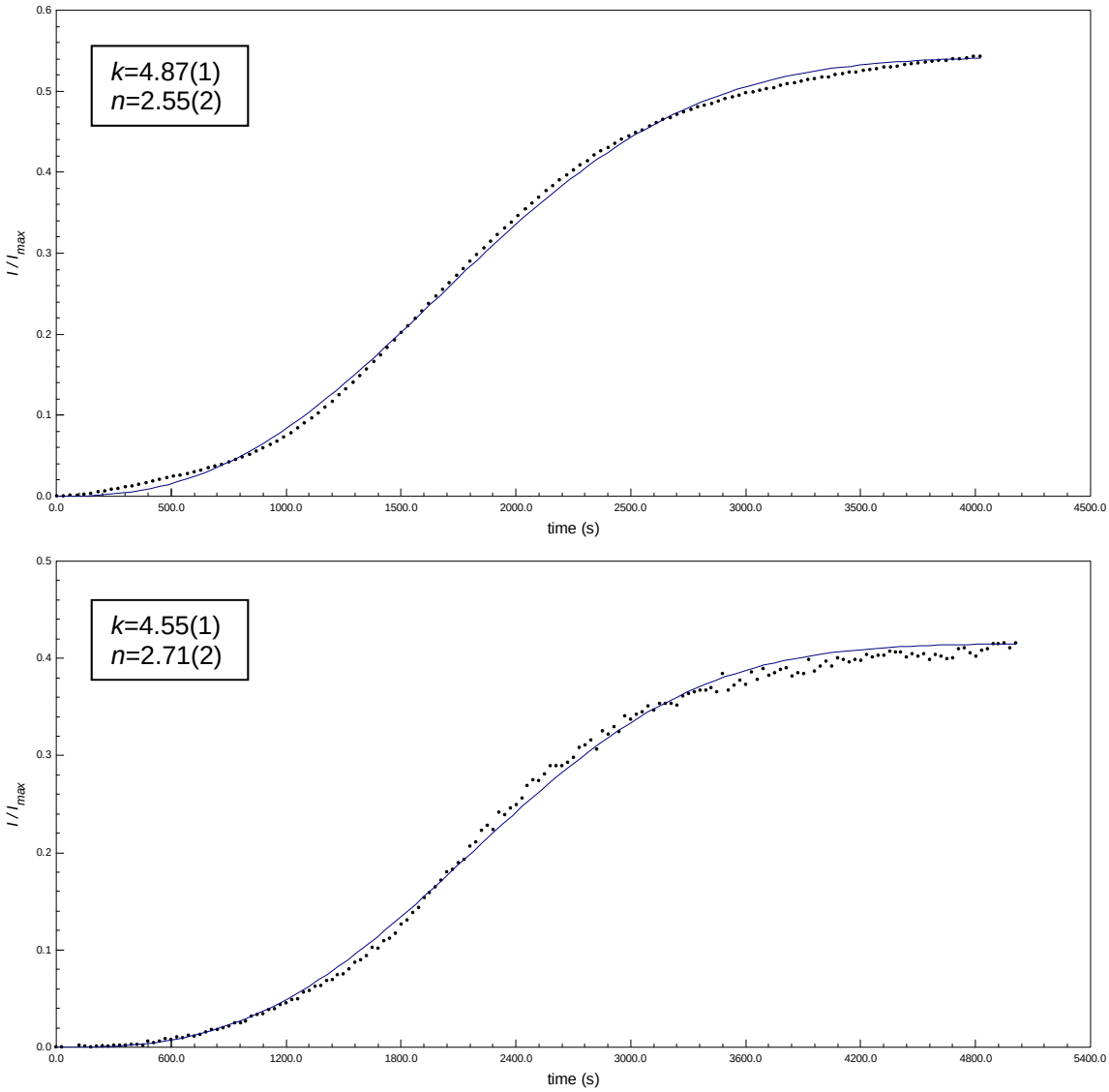

Fig. S11 Non-linear fit of the sigmoidal fluorescence emission data to a general JMAEK model for the transformation of amorphous indomethacin sample with particle size >75 μm. Fluorescence data was collected from: (top) sample top and (bottom) sample bottom.

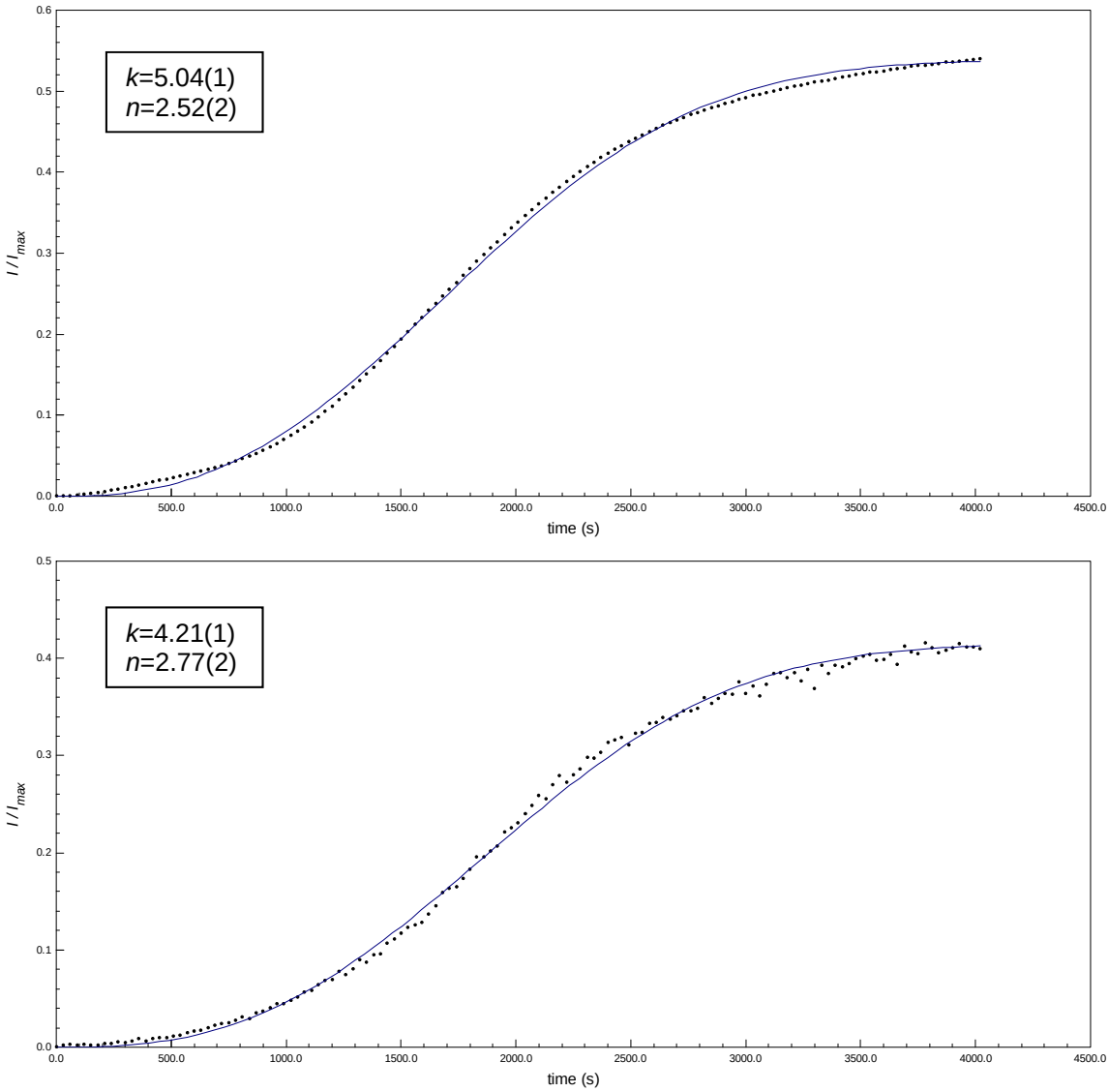

Fig. S12 Non-linear fit of the sigmoidal fluorescence emission data to a general JMAEK model for the transformation of another amorphous indomethacin sample with particle size >75 μm. Fluorescence data was collected from: (top) sample top and (bottom) sample bottom.

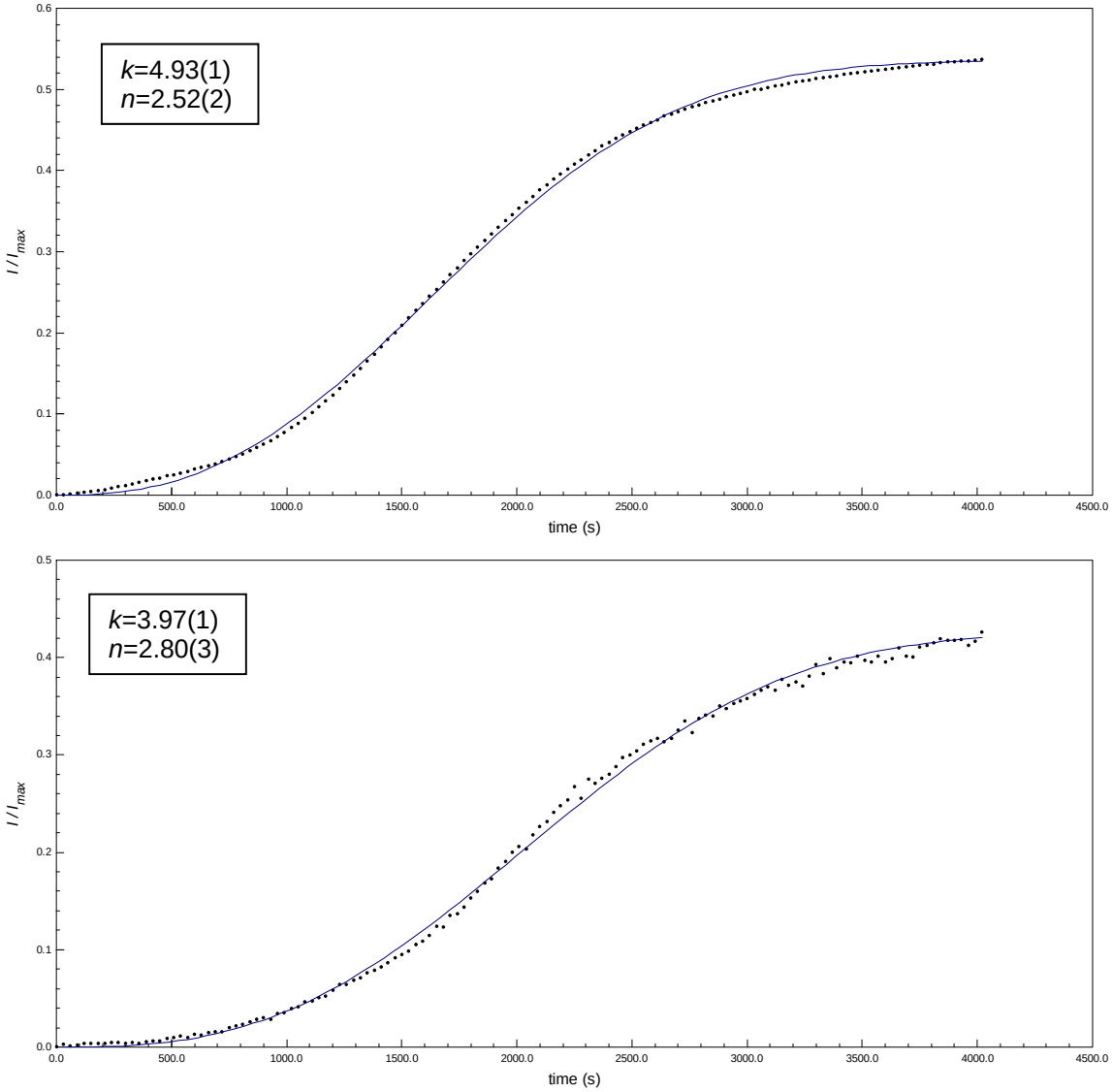

Fig. S13 Non-linear fit of the sigmoidal fluorescence emission data to a general JMAEK model for the transformation of a third amorphous indomethacin sample with particle size >75 μm. Fluorescence data was collected from: (top) sample top and (bottom) sample bottom.

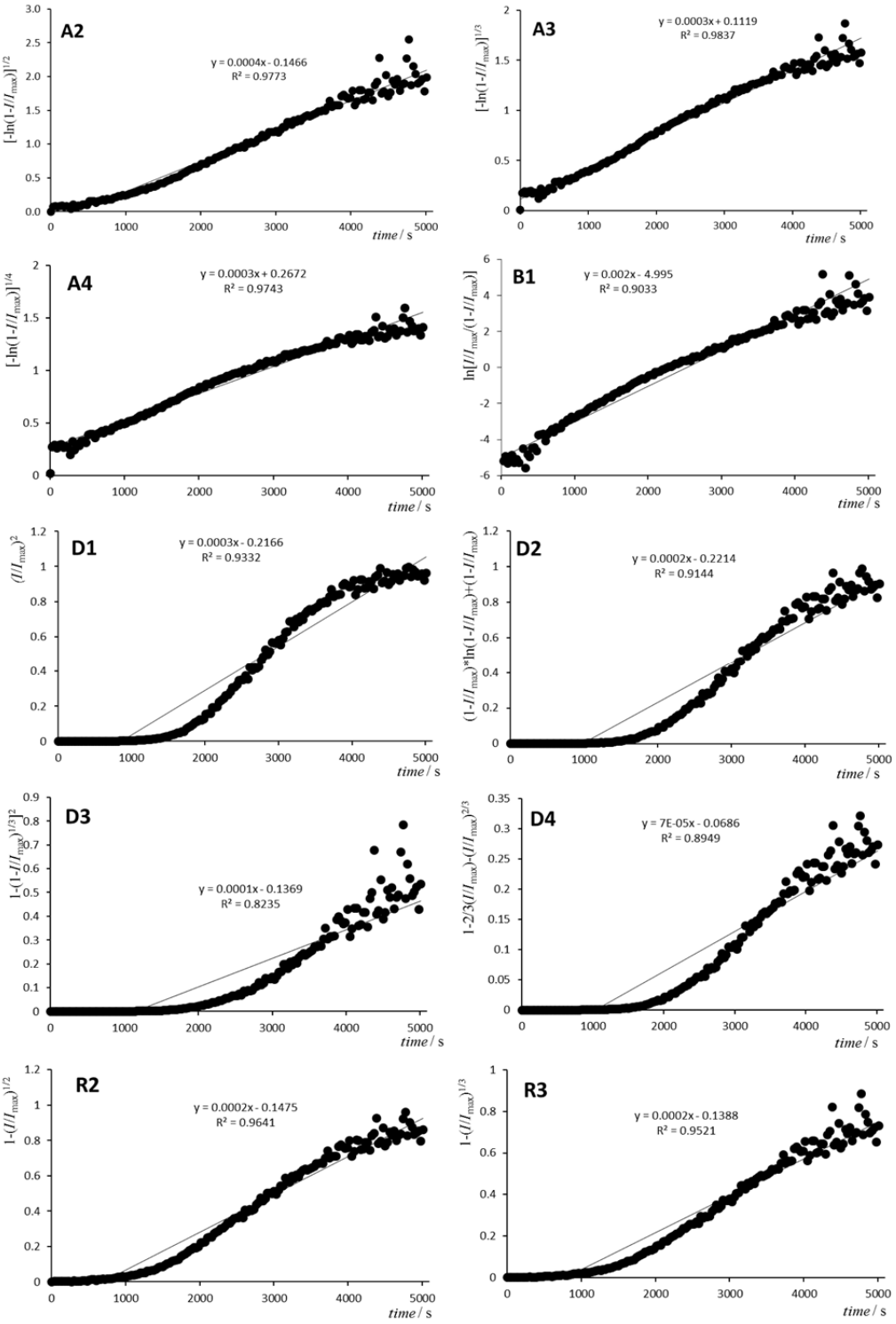

Fig. S14 Example of fitting the linearised $\frac{I}{I_{max}}$ fluorescence data for crystallization of amorphous indomethacin to ten different models of solid-state reactivity: (a) the **A2** model; (b) the **A3** model; (c) the **A4** model; (d) the **B1** Prout-Tompkins model; (e) the **D1** model; (f) the **D2** model; (g) the **D3** model; (h) the **D4** model; (i) the **R2** model; (j) the **R3** model. Sample was composed of particles with sizes 38 μm-53 μm and data was collected off the bottom sample surface.

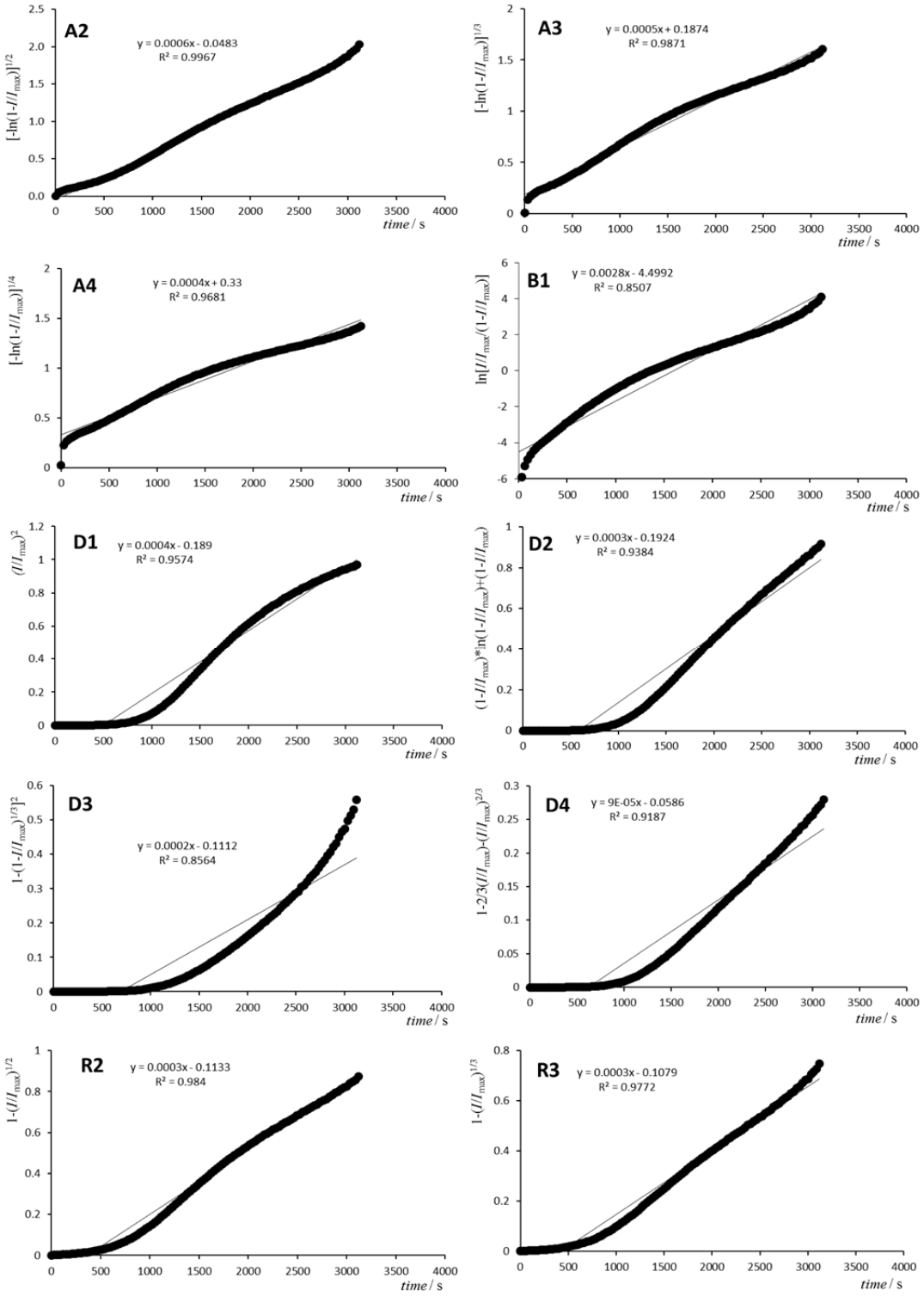

Fig. S15 Example of fitting the linearised $\frac{I}{I_{max}}$ fluorescence data for crystallization of amorphous indomethacin to ten different models of solid-state reactivity: (a) the **A2** model; (b) the **A3** model; (c) the **A4** model; (d) the **B1** Prout-Tompkins model; (e) the **D1** model; (f) the **D2** model; (g) the **D3** model; (h) the **D4** model; (i) the **R2** model; (j) the **R3** model. Sample was composed of particles with sizes 38 μm-53 μm and data was collected off the top sample surface.

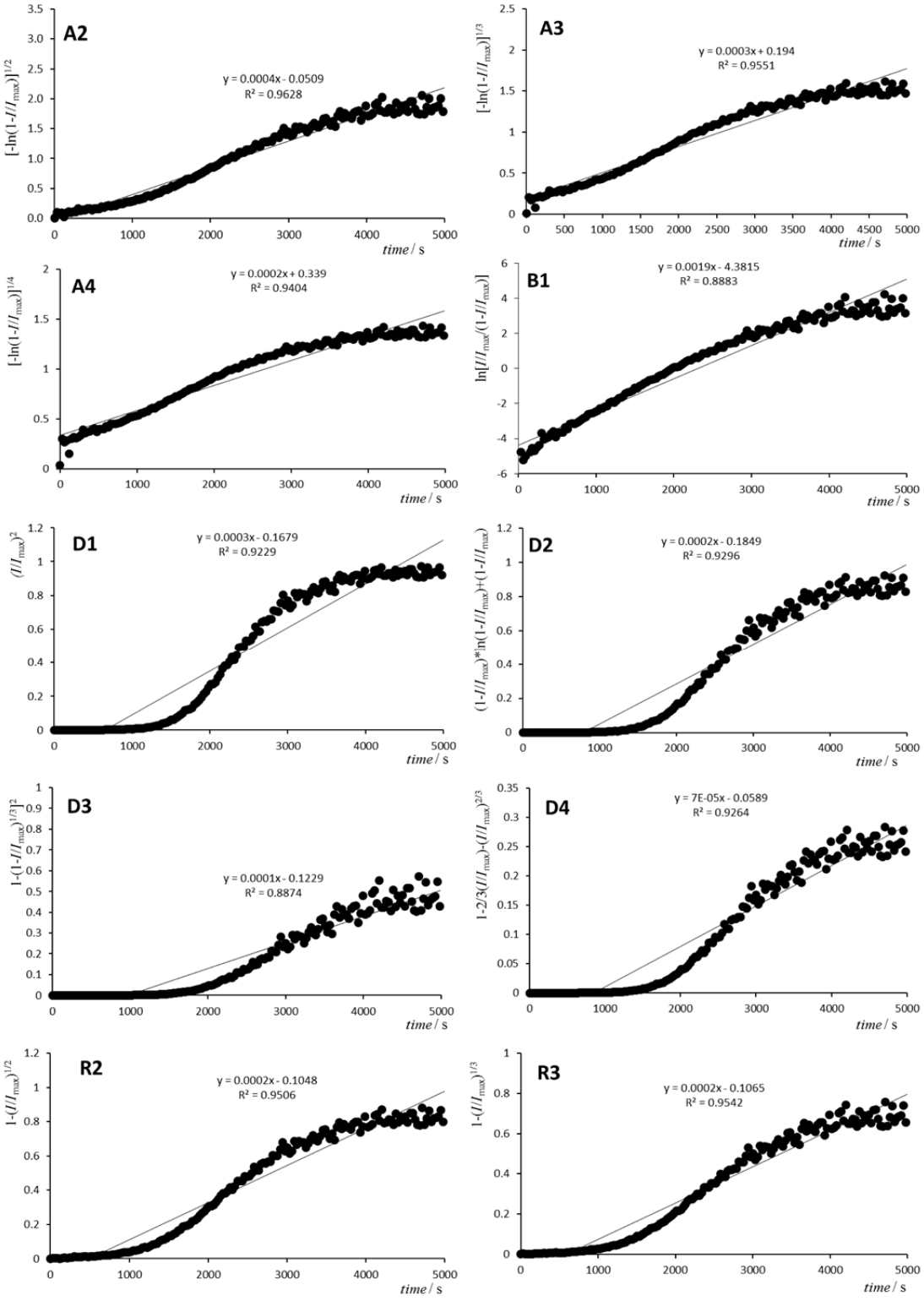

Fig. S16 Example of fitting the linearised $\frac{I}{I_{max}}$ fluorescence data for crystallization of amorphous indomethacin to ten different models of solid-state reactivity: (a) the **A2** model; (b) the **A3** model; (c) the **A4** model; (d) the **B1** Prout-Tompkins model; (e) the **D1** model; (f) the **D2** model; (g) the **D3** model; (h) the **D4** model; (i) the **R2** model; (j) the **R3** model. Like the sample in Fig. 14, this sample was also composed of particles with sizes 38 μm-53 μm and data was collected off the bottom sample surface.

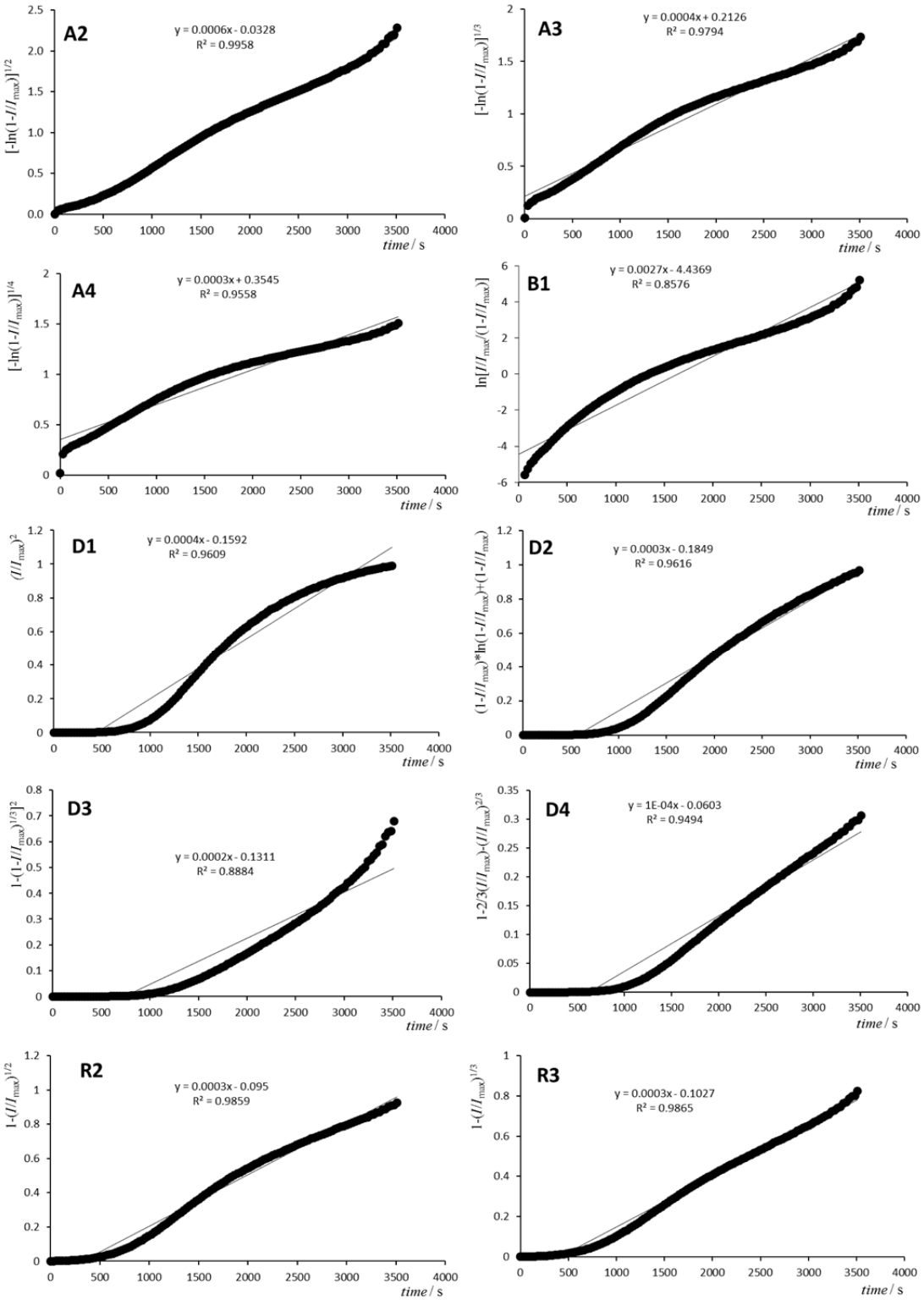

Fig. S17 Example of fitting the linearised $\frac{I}{I_{max}}$ fluorescence data for crystallization of amorphous indomethacin to ten different models of solid-state reactivity: (a) the **A2** model; (b) the **A3** model; (c) the **A4** model; (d) the **B1** Prout-Tompkins model; (e) the **D1** model; (f) the **D2** model; (g) the **D3** model; (h) the **D4** model; (i) the **R2** model; (j) the **R3** model. Like the sample in Fig. 15, this sample was also composed of particles with sizes 38 μm-53 μm and data was collected off the top sample surface.

1.6 Structures of relevant indomethacin solid forms

Crystal structures for all indomethacin solid forms studied in this work have been previously reported except, of course, the amorphous form. We attempted to understand the effect of structure on the observed fluorescence properties, but were so far unable to correlate any of the molecular structure parameters to fluorescence behaviour. In particular, we examined the potential variation of the fluorescence emission maximum wavelength and intensity with respect to four structural parameters: the amide N-CO bond distance (N-CO), the amide C=O double bond distance (C=O), the dihedral angle between the amide moiety and the 4-chlorophenyl substituent (Ph-CO angle) and the dihedral angle between the C and N atoms of the amide bond (N-CO angle). These parameters are illustrated in Fig. S18 and their comparison with fluorescence properties is given in Table 1. Computational chemistry investigations are underway to calculate the relationship between structure and spectroscopy in this system.

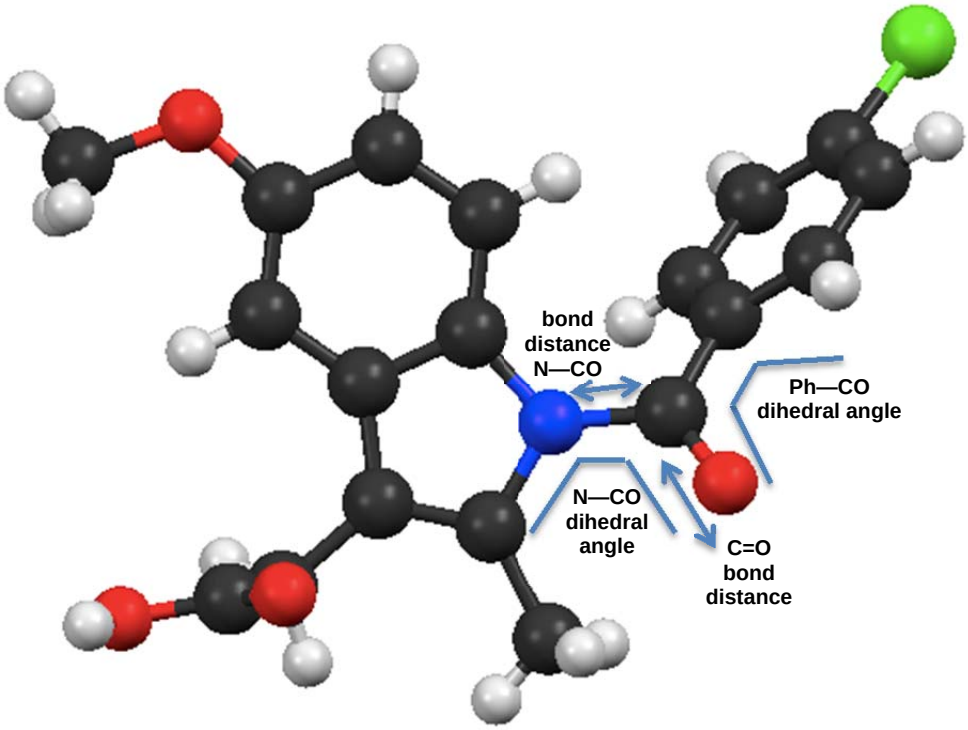

Fig. S18 Illustration of the four structural parameters investigated with respect to differences in fluorescence behaviour of different indomethacin solid forms.

Table S1. Comparison of selected parameters of indomethacin molecular structure with fluorescence properties for selected indomethacin solid forms

Solid Form	Appearance	λ_{max} (nm)	Intensity (relative to 390 nm excitation)	N—CO angle (°)	C=O distance (Å)	N—CO distance (Å)	Ph—CO angle (°)
γ (1972, RT)[a]	white	465	100	25.4	1.207	1.416	39.3
γ (1976, RT)[b]	white			26.2	1.206	1.417	40.3
γ (2003, 120 K)[c]	white			25.8	1.216	1.410	38.7
α (2002, RT)[d] molecule 1 molecule 2 molecule 3	white	500	32	 21.4 23.2 20.3	 1.204 1.221 1.226	 1.391 1.403 1.371	 50.0 51.9 52.9
saccharin cocrystal[e]	white	486	98-110	20.1	1.219	1.394	41.6
methanol solvate[f]	yellow	520	27	22.5	1.217	1.396	42.3
amorphous	yellow	520	26	-	-	-	-

a) CSD code INDMET, room temperature data; b) CSD code INDMET01, room temperature data; c) CSD code INDMET03, data at 120 K; d) INDMET02, room temperature data, three molecules per asymmetric unit; e) CSD code UFERED; f) CSD code BANMUZ.

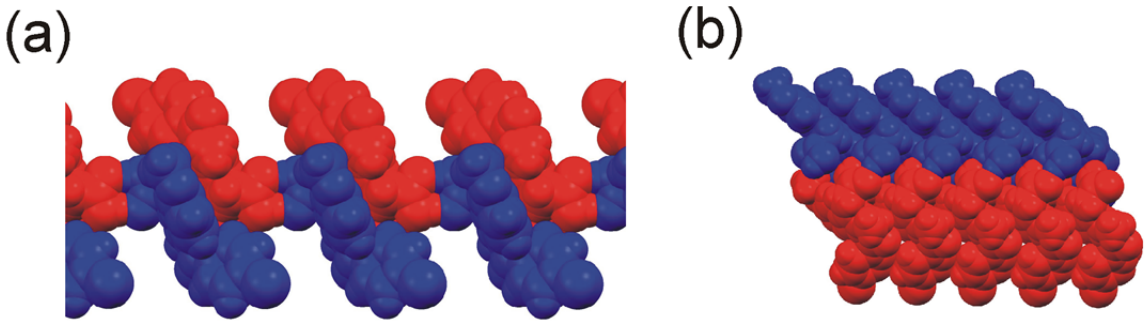

Fig. S19 Comparison of crystal packing of molecules in: (a) γ-indomethacin and (b) α-indomethacin. Different orientations of molecules are colour-coded, demonstrating the formation of head-to-tail stacks in the γ-form and head-to-head stacked molecules in the α-form.

Fragments of the crystal structure (with hydrogen atoms omitted for clarity), CSD reference code and literature references for single crystal structures of the indomethacin solid forms used in this study:

γ-indomethacin

INDMET, T. J. Kistenmacher and R. E. Marsh, *J. Am. Chem. Soc.* 1972, **94**, 1340.
INDMET01, Z. Galdecki and M. L. Glowka, *Rocz. Chem.* 1976, **50**, 1139.
INDMET03, P. J. Cox and P. L. Manson, *Acta Crystallogr.* 2003, **E59**, o986.

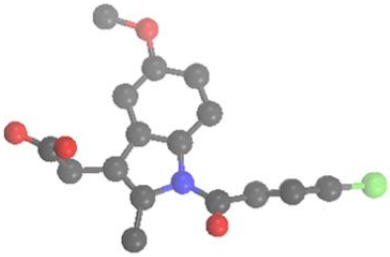

α-indomethacin

INDMET02, X. Chen, K. R. Morris, U. J. Griesser, S. R. Byrn and J. G. Stowell, *J. Am. Chem. Soc.* 2002, **124**, 15012

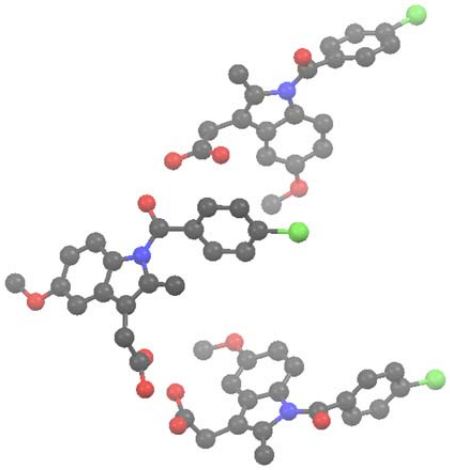

saccharin-indomethacin co-crystal

UFERED, S. P. Velaga, S. Basavoju and D. Bostrom, *Pharm. Res.* 2008, **25**, 530

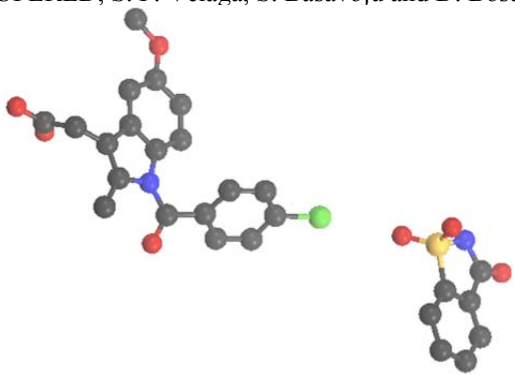

methanol solvate

BANMUZ, J. G. Stowell, S. R. Byrn, G. Zografi and M. Yoshioka, private communication, 2002.

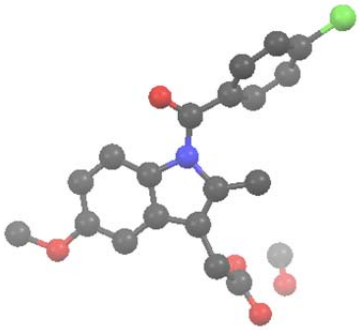

References

1) M. Yoshioka, B. C. Hancock and G. Zografi, *J. Pharm. Sci.* 1994, **83**, 1700.
2) N. Kaneniwa, M. Otsuka and T. Hayashi, *Chem. Pharm. Bull.* 1985, **33,** 3447**.**
3) M. S. Bernstein and M. A. Evans, *J. Chromatogr.* 1982, **229,** 179.
4) S. Basavoju, D. Boström and S. P. Velaga, *Pharmaceutical Research*, 2008, **25**, 530.
5) K. J . Crowley and G. Zografi, *J. Pharm. Sci.*, 2002, **91**, 492.